Oxygen transport and release of adenosine triphosphate in micro-channels and arterioles in the human microcirculation

Terry E. Moschandreou
Western University
Department of Applied Mathematics
London, Ontario
Canada

Corresponding author: Terry E. Moschandreou, Western University, Department of Applied Mathematics, London,Canada,tmoschan@uwo.ca

PeerJ PrePrints

Abstract

The governing nonlinear equations for oxygen transport and ATP concentration in a microfluidic channel and tube are solved with the aid of Maple and COMSOL Multiphysics simulation software. Considering a cell-rich and cell free region with RBCs and blood plasma, we obtain results showing clearly that there is a significant decrease in oxygen tension in the vicinity of an oxygen permeable membrane placed midway on the upper channel/tube wall and to the right side of it in the downstream field. The purpose of the membrane is to cause a rapid change in oxygen saturation as RBC's flow through channel/tube. To the right of the membrane downstream the greatest amount of ATP is released. It is shown that for smaller arterioles there is an optimal size for which greater amounts of ATP can be released. Finally the corresponding time-dependent oxygen transport problem for plug flow in a channel, which has not been simulated in previous models in the literature, is analyzed and different starting times are shown for ATP release at different points in the channel. The FE modelling is very accurate: The time evolution problem is modelled and solved in it`s entirety with exact parameters used in the literature for blood flow and oxygen transport in the microcirculation. A comparison is made between the steady state and time dependent solutions in order to validate the results. The implications of the time dependent model for biological systems such as the human microcirculation requires exact information on release of energy as ATP is released from blood cells and the present work is important in providing this information.

PeerJ PrePrints | http://dx.doi.org/10.7287/peerj.preprints.443v3 | CC-BY 4.0 Open Access | received: 12 Aug 2014, published: 12 Aug

1.Introduction

ATP is made up of Adenine, Ribose and Phosphate groups. It is the molecule of most organisms to transfer energy. Adenine is one of the bases found in DNA and RNA. Ribose is a sugar molecule found in RNA. There exist high energy bonds between the phosphates. Breaking the first high energy bond in ATP releases energy and a free phosphate. This energy is used to power cellular activities. What is left with 2 phosphates and Adenosine is called Adenine diphosphate or ADP. Energy from the breakdown of food is used to change the ADP to an ATP molecule. In cells, mitochondria supply the major portion of ATP consumed in the cystol. ADP-ATP translocation in mitochondria is studied by Klingenberg [1]. Mitchell [2] proposed that electron transport and ATP synthesis are related by a proton gradient across the inner mitochondrial membrane. A mechanism for microvascular blood flow regulation that is under current investigation depends on the oxygen saturation-dependent release by red blood cells (RBCs) of the signaling molecule ATP [3,4]. Increased RBC ATP release due to decreased O2 saturation results in a vasodilation signal that conducts upward through the microvascular tree. This signal can originate in arterioles, capillaries or venules. It is arterioles that the present work focuses on. Moschandreou et al. [5] have presented a theoretical model for steady-state radial and longitudinal oxygen transport in arterioles containing plasma and red blood cells and surrounded by living tissue. The governing equations were solved in a cell-rich and cell-free region. Using the transport equations for O_2 transport in [5] together with ATP concentration equations in [6,7], both defined in a micro-channel and then applied to representative arterioles, important information is obtained about ATP release. 3D printed microfluidic devices have been recently used to collect ATP while simultaneously measuring the release stimulus which is the reduced oxygen concentration [8,9]. RBC-derived ATP is measured when a luciferin luciferase mixture is applied and resulting chemiluminescence is determined. [10,11]

In the present paper a solution method is used to determine the oxygen tension and concentration of ATP in a microfluidic channel with dimensions, inlet and boundary conditions given by Sove et al.[6], then solve the governing equations of oxygen and ATP transport in tubes of different diameters and finally present the corresponding time-dependent solution in a channel with plug flow. Three objectives of the present work is to provide a compact and accessible method of solution in Maple[12], secondly to include a realistic model of blood flow in arterioles(tubes) calculating the oxygen transport and concentration of ATP produced due to a change in oxygen saturation and finally solve the corresponding time dependent problem using COMSOL Multiphysics [13] which will predict the onset times of ATP in the channel.

PeerJ Preprints

PeerJ PrePrints | http://dx.doi.org/10.7287/peerj.preprints.443v3 | CC-BY 4.0 Open Access | received: 12 Aug 2014, published: 12 Aug

2.Materials and Methods

2.1 Channel Flow and Oxygen Transport

Hellums and co-workers [14,15,16] have developed a model for intraluminal oxygen transport in arteriole size vessels.

We adopt this model for square channel flow where Equation (1) is used below to model oxygen transport in a micro-fluidic device.

The geometry of the present mathematical model is shown in Figure 1.

PeerJ PrePrints

PeerJ PrePrints | http://dx.doi.org/10.7287/peerj.preprints.443v3 | CC-BY 4.0 Open Access | received: 12 Aug 2014, published: 12 Aug

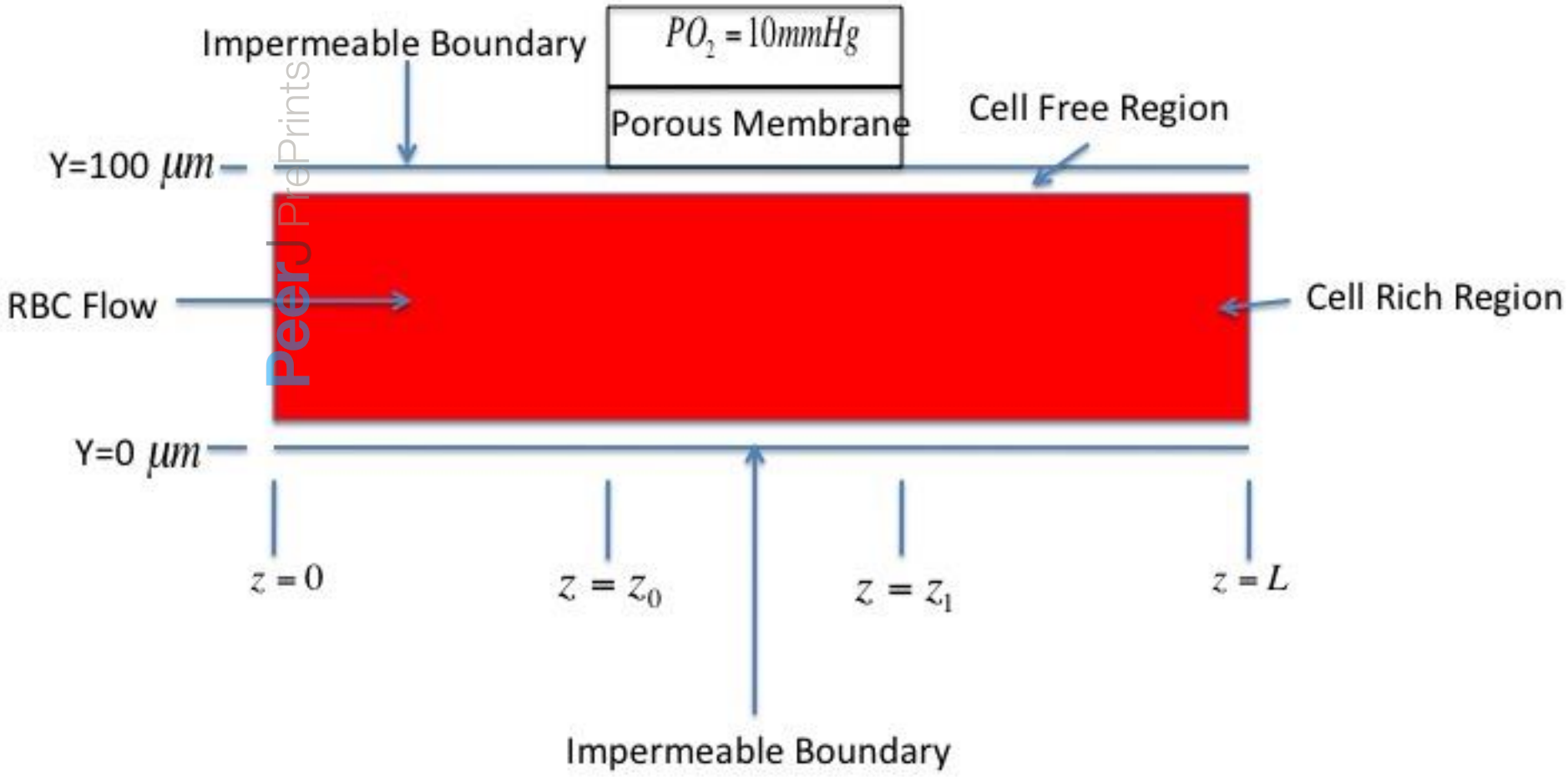

PeerJ PrePrints

PeerJ PrePrints | http://dx.doi.org/10.7287/peerj.preprints.443v3 | CC-BY 4.0 Open Access | received: 12 Aug 2014, published: 12 Aug

Figure 1

Geometry of mathematical model used for channel flow

$$\left(v_p(1-H_T)+v_{RBC}H_T\frac{K_{RBC}}{K_p}\left(1+\frac{[Hb_T]}{K_{RBC}}\frac{dSO_2}{dPO_2}\right)\right)\frac{\partial PO_2}{\partial z}=D_p\frac{\partial^2 PO_2}{\partial y^2} \quad (1)$$

There is a core region of blood flow with RBCs and plasma and a cell-free region with only plasma flowing as shown in Figure 1. The blood plasma velocity is v_p and v_{RBC} is the velocity of RBCs with plasma in the cell-rich region. The velocity of the RBCs is lower due to the slip between plasma and RBCs.[17] . There is a reduction of red cell transit time through a given tube segment known as tube hematocrit H_T. The discharge hematocrit, is the hematocrit of blood entering or leaving the tube segment. Dynamic hematocrit reduction is known as the Fahraeus effect. [18] In blood vessels with diameters less than 500 microns both the hematocrit decreases with decreasing vessel diameter.

The distribution of RBC`s is such that hematocrit is higher at the center of the channel and lower near the wall. [5] . The term $\frac{dSO_2}{dPO_2}$ is the slope of the oxyhemoglobin dissociation curve and is a nonlinear function of PO_2. (Nair et al. [15,16]) The dissociation curve is approximated by the Hill equation in Eq. (1a) , where N is an empirical constant and P_{50} is the oxygen tension that yields 50 % oxygen saturation. $[Hb_T]$ is the total heme concentration which is equal to four times the hemoglobin concentration due to fact that there are four heme groups on each hemoglobin molecule. D_p is the oxygen diffusion coefficient in plasma and has units of $\mu m^2/s$, and K_{RBC} and K_p are the solubilities of O_2 in the RBCs and plasma, respectively, and have units of M/mmHg. Differentiating the Hill equation with respect to PO_2 gives Eq. (1b).

$$SO_2(y,z)=\frac{PO_2{}^N(y,z)}{PO_2{}^N(y,z)+P_{50}{}^N} \quad (1a)$$

$$\frac{dSO_2}{dPO_2}=\frac{NP_{50}^N\,PO_2^{N-1}}{\left(P_{50}^N+PO_2^N\right)^2} \quad (1b)$$

PeerJ PrePrints | http://dx.doi.org/10.7287/peerj.preprints.443v3 | CC-BY 4.0 Open Access | received: 12 Aug 2014, published: 12 Aug

Generally blood flow velocity varies from zero at the wall of the channel to maximum at center. In [19] a quoted value of arteriole flow velocity is in the range of 1 to 1.275 mm/s (1000 to 1275 microns/s). For discharge hematocrits of about 0.4 we have used a value of 0.7 for the ratio of tube hematocrit to discharge hematocrit.[18,20] These values in [18,20] are assumed for arterioles of diameter 20 down to 10 microns. We have used a representative value for discharge hematocrits of 0.4 for channel and tube flow ranging from 100 down to 10 microns radius.

Equation (2) governs oxygen transport in the cell-free plasma layer,

$$v_p \frac{\partial PO_2}{\partial z} = D_p \frac{\partial^2 PO_2}{\partial y^2} \tag{2}$$

PeerJ PrePrints

2.2 Channel Flow and ATP Model

ATP concentration given by C_{ATP} is governed by the following transport equation.

$$v_p \frac{\partial C_{ATP}}{\partial z}(1-H_T) = D_{ATP} \frac{\partial^2 C_{ATP}}{\partial y^2}(1-H_T) + R \cdot H_T - k_t C_{ATP}(1-H_T) \tag{3}$$

where D_{ATP} is the diffusion coefficient of ATP in blood plasma with units of $\mu m^2/s$ and k_t is a concentration rate constant with units of s^{-1}.

Equations (1) and (3) are coupled partial differential equations through the nonlinear function R(y,z) [6],[21],

$$R(y,z) = -14 \cdot SO_2(y,z) + 14 \quad , \tag{4}$$

where,

$$SO_2(y,z) = \frac{PO_2{}^{2.7}(y,z)}{PO_2{}^{2.7}(y,z) + 3600^{2.7}} \tag{5}$$

PeerJ PrePrints | http://dx.doi.org/10.7287/peerj.preprints.443v3 | CC-BY 4.0 Open Access | received: 12 Aug 2014, published: 12 Aug

and a maximum ATP release rate of 14 $\mu M / s$.[6]

Equations 1 and 3 are solved using Maple 13 [12].

PeerJ PrePrints

2.3 Channel Inlet and Boundary Conditions for Oxygen Transport and ATP Concentration

The inlet conditions for both oxygen tension and ATP concentration at the entrance to the channel where the oxygen porous membrane is located at z=7000 microns are given by Equation 6:

$$PO_2(y,7000) = P_0 = 150\, mmHg$$

$$C_{ATP}(y,7000) = C_0 = 0\ \mu M \qquad (6)$$

The boundary conditions for both oxygen tension and ATP concentration in the channel are given by Equation 7:

$$\frac{\partial PO_2}{\partial y}(h,z) = 0 \qquad 0 \le z < z_0,\ z_1 < z \le L$$

$$\frac{\partial PO_2}{\partial y}(-h,z) = 0 \qquad 0 \le z \le L$$

PeerJ PrePrints | http://dx.doi.org/10.7287/peerj.preprints.443v3 | CC-BY 4.0 Open Access | received: 12 Aug 2014, published: 12 Aug

$$D_p K_p \frac{\partial PO_2}{\partial y}(h,z) = D_m K_m \frac{PO_{2(PM)} - PO_2(h,z)}{\tau} \qquad z_0 \le z \le z_1 \tag{7}$$

$$\frac{\partial C_{ATP}}{\partial y}(h,z) = 0 \qquad z_0 \le z \le z_1$$

$$\frac{\partial C_{ATP}}{\partial y}(-h,z) = 0 \qquad z_0 \le z \le z_1$$

PeerJ PrePrints

TABLE 1 Model Parameters

Physical parameters used in oxygen transport model.

Blood plasma velocity	$v_p\ (\mu m/s)$	1275[19]
Red Blood Cell velocity	$v_{RBC}\ \mu m/s$	1147.5 [19]
Slip coefficient	slp	0.1 [17]
Discharge Hematocrit	H_D	0.4 [18,20]
Tube Hematocrit	H_T	0.28 [18,20]
O_2 Diffusivity in plasma	$D_p\ (\mu m^2/s)$	2750[5],[6]
O_2 Diffusivity in O_2 Permeable Membrane	$D_m\ (\mu m^2/s)$	160000[6]
Plasma Layer Thickness	T(μm)	1[6]

PeerJ PrePrints | http://dx.doi.org/10.7287/peerj.preprints.443v3 | CC-BY 4.0 Open Access | received: 12 Aug 2014, published: 12 Aug

O_2 Permeable Membrane PO_2	$PO_{2(PM)}$(mmHg)	10[6]
Axial position for start of O_2 Permeable Membrane along channel/arteriole	$z_0(\mu m)$	7000 [6]
Axial position for end of O_2 Permeable Membrane along channel/arteriole	$z_1(\mu m)$	7700[6]
Inlet PO_2	P_0 (mmHg)	150 [6]
Microfluidic Device/Arteriole length	L (μm)	14700
O_2 Porous Membrane Thickness	$\tau(\mu m)$	100 [6]
Hill Coefficient	N	2.7[5]
O_2 Solubility in Porous Membrane	$K_m(\frac{\mu M}{mmHg})$	17.959[6]
O_2 Solubility in Plasma	$K_p(\frac{\mu M}{mmHg})$	1.33[5],[6]
O_2 Solubility in RBCs	$K_{RBC}(\frac{\mu M}{mmHg})$	1.47 [5],[6]
Reaction Rate	K_t s^{-1}	0.1 [6]

PeerJ PrePrints

PeerJ PrePrints | http://dx.doi.org/10.7287/peerj.preprints.443v3 | CC-BY 4.0 Open Access | received: 12 Aug 2014, published: 12 Aug

Total Heme Concentration	$[Hb_T]\,(\mu M)$	5350 [5],[6]
ATP Diffusivity in plasma	$D_{ATP}\ (\mu m^2/s)$	475 [6]
Partial Pressure at 50% Saturation	$P_{50}\,(\text{mmHg})$	27 [5],[6]

PeerJ PrePrints

2.4 Tube Flow and Oxygen Transport and ATP Concentration

In arteriolar(tube) flow Equation (8) is used below to model oxygen transport. The model used includes a realistic diffusive oxygen transport term.

Wheras a channel is considered in [6],the inclusion of an extra radial term is used in the present work to effectively model arteriolar oxygen transport.

$$\left(v_p(1-H_T)+v_{RBC}H_T\frac{K_{RBC}}{K_p}\left(1+\frac{[Hb_T]}{K_{RBC}}\frac{dSO_2}{dPO_2}\right)\right)\frac{\partial PO_2}{\partial z}=D_p\left(\frac{\partial^2 PO_2}{\partial y^2}+\frac{1}{y}\frac{\partial PO_2}{\partial y}\right) \tag{8}$$

Same inlet and boundary conditions are used here as in channel flow in section 2.3. A tangent surface on the top of tube defines the boundary condition as in channel flow which acts along a line on the top of the surface of the tube as shown in Figure 2.

PeerJ PrePrints | http://dx.doi.org/10.7287/peerj.preprints.443v3 | CC-BY 4.0 Open Access | received: 12 Aug 2014, published: 12 Aug

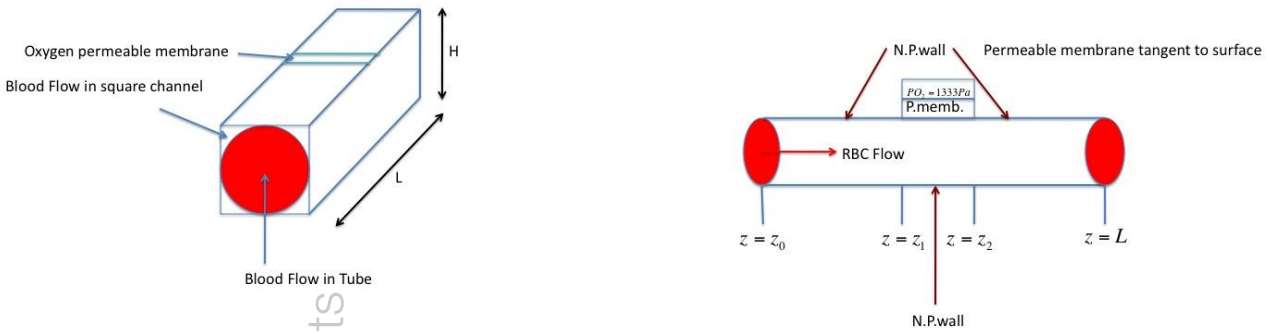

Figure 2

Geometry of Model Used for Tube Flow

ATP concentration in a tube given by C_{ATP} is governed by the following transport equation.

$$v_p \frac{\partial C_{ATP}}{\partial z}(1-H_T) = D_{ATP}\left(\frac{\partial^2 C_{ATP}}{\partial y^2} + \frac{1}{y}\frac{\partial C_{ATP}}{\partial y}\right)(1-H_T) + R \cdot H_T - k_t C_{ATP}(1-H_T) \quad (9)$$

where D_{ATP} is the diffusion coefficient of ATP in blood plasma and k_t is the concentration rate constant defined previously.

2.5 Parabolic Flow in Tubes of Radius R=10, 20 Microns

PeerJ PrePrints | http://dx.doi.org/10.7287/peerj.preprints.443v3 | CC-BY 4.0 Open Access | received: 12 Aug 2014, published: 12 Aug

Convective transport in the cell-free (plasma) and cell-rich (RBCs) regions involves specific assumed velocity profiles.

See Appendix A for the blood plasma velocity, v_p, given by Equation (A1). The RBC velocity in the cell-rich region is given by Equation (10),

$$v_{RBC} = v_p(1 - slp) \tag{10}$$

where slp is given in Table 1.

The boundary conditions used in the simulations are given by Eqs. (6) and (7) with a note that the radial derivative involves a singular coefficient and is treated separately in the Maple coding. Here the derivative is at y=0 where y denotes the radial coordinate in Eq. (9).

PeerJ PrePrints

2.6 Time Dependent Channel Flow

The governing equations for time dependent erythrocytic flow in a microfluidic channel are given by the following[22,23] :

PeerJ PrePrints | http://dx.doi.org/10.7287/peerj.preprints.443v3 | CC-BY 4.0 Open Access | received: 12 Aug 2014, published: 12 Aug

$$\left(H_T C_{Hb}\frac{\partial SO_2}{\partial PO_2}\right)\frac{\partial PO_2}{\partial t}+\left(v_p(1-H_T)+v_{RBC}H_T\frac{K_{RBC}}{K_P}\cdot\left(1+\frac{[Hb_T]}{K_{RBC}}\right)\cdot\frac{\partial SO_2}{\partial PO_2}\right)$$
$$\times\frac{\partial PO_2}{\partial z}=\xi\cdot j_{wall}+D_p\cdot\left(\frac{\partial^2 PO_2}{\partial y^2}+\frac{\partial^2 PO_2}{\partial z^2}\right)=2750\cdot\eta\cdot\left.\frac{\partial PO_2}{\partial y}\right|_{y=H}+D_p\cdot\left(\frac{\partial^2 PO_2}{\partial y^2}+\frac{\partial^2 PO_2}{\partial z^2}\right) \quad (11)$$

COMSOL Multiphysics [13] is used to handle Eq. (11).

In order to set the mass coefficient to units of seconds, we rewrote the units as ,

$$\frac{\mu m^2}{s}\cdot\frac{s^3}{kg}=\cdot\frac{\mu m^2}{s}\cdot\frac{1}{kg/s}\cdot s^2 \quad (12)$$

and used a flow rate of 7.8 microlitres/min [6]. Converting to kg/s a factor of approximately 0.5×10^8 was introduced in mass coefficient in COMSOL. This was set since the units of Γ and f (Appendix B) were independent of kg/s.(ie cancellation of pascal units).

PeerJ PrePrints

3. Numerical Methods

3.1 Maple Solution Scheme

The default method is used in Maple 13 [12] which uses a second order(in radial or y direction and axial direction z) centered, implicit finite difference scheme to obtain the solution. The number of points in the stencil of finite difference scheme is one greater than the order of each equation. A first order accurate boundary condition is used for a second order accurate method and still produces a solution of second order accuracy.

Derivatives in the initial/boundary conditions are specified in indexed D notation.($D_p K_p D_1(PO_2)(20,x)=D_m K_m\frac{10-PO_2(20,x)}{\tau}$ is the boundary condition along oxygen porous membrane.) The calling sequence in Maple is pdsolve(PDE,conditions,numeric,options). The parameters include the type of PDE which allows for a single z-dependent partial differential equation in one independent variable y, and the set of initial and boundary conditions given by Eq. (6) and (7). A numeric keyword is used to invoke a centered, implicit finite difference scheme and options specifies the spacing of the spatial points on the discrete mesh on which solution computes and defaults to 1/20 th of the spatial range of problem.

PeerJ PrePrints | http://dx.doi.org/10.7287/peerj.preprints.443v3 | CC-BY 4.0 Open Access | received: 12 Aug 2014, published: 12 Aug

Case 1

In maple the following commands are used.

pds:= pdsolve(sys,IBC,numeric)

$$IBC := \{PO_2(y,7000) = 150, D_1(PO_2)(0,z) = 0, D_1(PO_2)(100,z) = 787 \cdot 0.1 - 787 \cdot 0.01 \cdot PO_2(100,z),$$
$$C_{ATP}(y,7000) = 0, D_1(C_{ATP})(100,z) = 0, D_1(C_{ATP})(0,z) = 0\} \quad (13)$$

The boundary conditions and entry conditions are such that the entry condition for blood flow is uniform oxygen tension of 150 mmHg at a length of 7000 microns from inlet of microfluidic device and a flux condition through permeable membrane shown in Figure 1, due to oxygen source at permeable wall at length $z = z_0 = 7000$ microns, height y=100 microns .[6] The oxygen flux through membrane was set above in definition of IBC between z_0 and z_1 in Fig(1).

The condition of oxygen impermeability between 0 and z_0 and z_1 and L is set in the IBC definition in Maple for both oxygen tension and ATP concentration. The novelty of present work is that in Maple the command pdsolve was used again to solve Equation 1 using the solution in Case 1 above as an entry condition for the region between z_1 and L (Fig 1) where a no flux condition or flux of zero is set in the definition of the boundary condition.

That is we have the following :

Case 2.

In Maple the solution obtained from Case1 is written as:

U:=subs(pds:-value(output=listprocedure), $PO_2(y,z)$); (14)

Proceeding in Maple language, Eq. 1 is defined as in Case 1 by defining the equation by a variable 'PDE'.

The entry and boundary conditions become as follows using the command given by Eq. (14):

$$IBC := \{PO_2(y,7700) = U(y,7700), D_1(PO_2)(0,z) = 0, D_1(PO_2)(100,z) = 0$$

PeerJ PrePrints | http://dx.doi.org/10.7287/peerj.preprints.443v3 | CC-BY 4.0 Open Access | received: 12 Aug 2014, published: 12 Aug

It can be observed that the solution obtained from Case 1 is used up to the end of the oxygen permeable wall and set to be an inlet condition in z to where the non-permeable wall condition starts to the right of the oxygen porous membrane.The advantage to store the solution in the computational field by using (14) is to solve the partial differential equations in two steps in the entire region from z=0 to z=L as shown in Figure 1.

3.2 COMSOL Multiphysics Solution Scheme

The General Form PDE Interface in COMSOL Multiphysics 4.3b [13] was used in time dependent simulations where the initial/boundary conditions were implemented as shown in Equation (6) and (7) with the addition of an initial condition in time (t=0) for PO_2 ,equal to 20kPa or equivalently 150 mmHg defined at every point in the channel. The general form is used in COMSOL for nonlinear PDE's and is appropriately set as follows. After piecing together three rectangles in COMSOL geometry interface due to permeable membrane and nonpermeable walls, the general form PDE defined on resulting domain is [13] shown in Appendix B.

Choosing options from PDE interface as ``Zero Flux`` and ``Flux/Source`` as well as ``Initial Values`` all boundary/initial values were specified as in Equation (6) and (7) above and condition at t=0 seconds.

As COMSOL Multiphysics is a finite-element method based software package[13], a physics-controlled mesh with extra fine element size was used in all simulations.

Finally the source term above was set to f and $e_a = 0$. Γ_x and Γ_y have units of N/m, f has units of Pa, and d_a has units of seconds. The boundary condition in COMSOL at oxygen permeable membrane is defined as,

$$-\mathbf{n}\cdot\Gamma = g - qu \tag{15}$$

where g is a boundary flux/source term and q is a boundary absorption term.

For the time dependent problem, the boundary condition at permeable membrane is,

$$D_p K_p \frac{\partial PO_2}{\partial y}(h,z,t) = D_m K_m \frac{PO_{2(PM)} - PO_2(h,z,t)}{\tau} \qquad z_0 \le z \le z_1$$

PeerJ PrePrints | http://dx.doi.org/10.7287/peerj.preprints.443v3 | CC-BY 4.0 Open Access | received: 12 Aug 2014, published: 12 Aug

and thus we take the same boundary condition in the COMSOL time dependent problem as in maple solution,

$g = 78.7 \times 1333.33$

$q = 7.87$

With these definitions Equations (1,13-14) , boundary conditions (6,7) and initial condition of 20 kPa at t=0 were input to COMSOL interface.

PeerJ PrePrints

4. Results and Discussion

Steady State and Time-Dependent Oxygen Transport and ATP Release in Micro-Channel and Tube

The computational model of O_2 transport and ATP concentration in a micro-channel and in an arteriole includes a more physiological equation that has been used before, that is, a radial and time-dependent transport equation. For different size arterioles, we calculated how the radially changing PO_2 inside the vessels decreases with increasing distance z downstream from the vessel inlet. Our calculations show appreciable drops in radial intraluminal PO_2 downstream from where the oxygen permeable boundary condition is set [6]. These results are similar to the results in [6], however in addition include realistic tube-like geometries, differently assumed velocity profiles and time dependent oxygen transport.

PeerJ PrePrints | http://dx.doi.org/10.7287/peerj.preprints.443v3 | CC-BY 4.0 Open Access | received: 12 Aug 2014, published: 12 Aug

For steady-state oxygen transport in a channel of radius 50 microns it is observed that the greatest decrease in oxygen tension is near the oxygen permeable membrane and to the right of it downstream and in Figure 3–A-2 an ATP concentration as large as 0.245 μM occurs 3 mm downstream from the membrane. Throughout the channel and downstream of membrane the ATP concentration flattens out at center of channel (y=0), and increases at ends of channel height from centerline. This parabolic behavior is similar to results in [6] as shown there in Figure 2-C. The ATP profiles for 6mm downstream from the membrane is shown in Figure 3-A-3 and directly in the membrane region at z=7700 microns as shown in Figure 3-A-1 Compiled profiles starting at end of membrane to the end of channel downstream are shown in Figure 3-B. In Figure 3-C, the oxygen tension is shown for values starting at z=7700 microns at membrane to values downstream ending at z=14700 microns. It is observed that the oxygen tension profiles flatten out downstream to a value of approximately 12800 Pa or 96 mmHg. The inlet value is in accordance to Sove's work [6] with a value of 150 mmHg and our results for the steady state problem in the channel is slightly more than Sove's value of 95 mmHg uniform across the height of channel and downstream at the end of the channel at z=L. It is concluded in Figure 3 (A-C) that there is a significant decrease in oxygen tension to the right of the permeable membrane downstream. It is in this region that there is significant concentration of ATP released by RBC's uniformly across the height of channel. The second part of the present work was to determine the onset time of the release of ATP and to show complete oxygen transport profiles with changes in time. It is shown in Figure 4 that starting at initial oxygen tension of 20000 Pa(150 mmHg) at time t=0 seconds, the oxygen tension in the channel evolves to the steady state solution. The solution asymptotically approaches the steady state oxygen tension near the steady state value of 12800 Pa which is approximately equal to the 96 mmHg value(Figure 3-C) obtained in the steady state solution computed above in Maple. This is seen by the constant shaded region to the right of the permeable membrane in Figure. 8. The complete time dependent transition profiles are shown starting with t=5e-5s in Figure 5 , t=0.005 s in Figure 6, t=0.01 s in Figure 7 and finally t=0.025s in Figure 8.

PeerJ Preprints

PeerJ PrePrints | http://dx.doi.org/10.7287/peerj.preprints.443v3 | CC-BY 4.0 Open Access | received: 12 Aug 2014, published: 12 Aug

PeerJ PrePrints

Conclusions

An approach to solve the governing equations of oxygen transport and ATP concentration in a microfluidic channel with a section of permeable wall subjected to a non-zero flux condition has been presented. The results clearly show that significant concentrations of ATP are released downstream and that the onset of ATP occur at various times from zero to 25 ms and where the steady and time-dependent solutions were validated by comparison. Future consideration for the present problem is to consider a network of micro-vessels and use powerful geometrical features of COMSOL Multiphysics to model and simulate ATP release in these connected micro-vessels of the microvasculature.

Acknowledgements

I would like to acknowledge Dr. Dan Goldman, for suggesting the present work to me and for the use of computer equipment to complete this paper.

PeerJ PrePrints | http://dx.doi.org/10.7287/peerj.preprints.443v3 | CC-BY 4.0 Open Access | received: 12 Aug 2014, published: 12 Aug

Appendix A

The following equation governs blood plasma velocity, [3]

$$v_p(y) = \frac{3 \cdot 130 \times 10^6 \frac{\mu m^3}{s}}{4 \cdot w\left(h^3 + \left(\frac{\mu_p}{\mu_c} - 1\right) y_i^3\right)} \begin{cases} (h^2 - y^2), & y_i \le y \le h \\ (h^2 - y_i^2) +_i \frac{\mu_p}{\mu_c}(y_i^2 - y^2), & 0 \le y \le y_i \end{cases}$$

where w is the width of the channel which in [6] is 1500 microns, y_i is 49 microns, h is 50 microns and $\frac{\mu_p}{\mu_c}$ is 1.26^{-1} as obtained from [20] for a tube of diameter 100 microns with hematocrit 0.2.

PeerJ PrePrints

PeerJ PrePrints | http://dx.doi.org/10.7287/peerj.preprints.443v3 | CC-BY 4.0 Open Access | received: 12 Aug 2014, published: 12 Aug

Appendix B

In eq. (13) we require that the derivative, $\partial S / \partial P$ be computed . Taking the derivative leads to the following equation, which we use in Eqs(B4,B6) and(B7) below,

PeerJ PrePrints

$$\frac{\partial S}{\partial P} = 2.7 \cdot 3600^{2.7} \cdot \frac{P^{1.7}}{(P^{2.7} + 3600^{2.7})^2} \tag{B1}$$

$$\nabla = \left[\frac{\partial}{\partial x}, \frac{\partial}{\partial y} \right] \tag{B2}$$

$$e_a \frac{\partial^2 u}{\partial t^2} + d_a \frac{\partial u}{\partial t} + \nabla \cdot \Gamma = f \tag{B3}$$

$$\Gamma_x = -2750 \cdot u_x / (1 \times 10^6) \tag{B4}$$

$$\Gamma_y = -2750 \cdot u_y / (1 \times 10^6) \tag{B5}$$

PeerJ PrePrints | http://dx.doi.org/10.7287/peerj.preprints.443v3 | CC-BY 4.0 Open Access | received: 12 Aug 2014, published: 12 Aug

$$f = -0.645\left[(50^2 - 49^2) + 0.79(49^2 - y^2)\right] \times 0.72 - 0.58 \times 0.28 \times \left[(50^2 - 49^2) + 0.79(49^2 - y^2)\right]\frac{1.47}{1.33} \times \left(1 + (0.5350/1e-4/1.47) \cdot \frac{\partial S}{\partial P}\right) \cdot u_x \quad \text{(B6)}$$

$$d_a = 0.28 \cdot 0.5 \times 10^8 \cdot 0.208 \cdot \frac{\partial S}{\partial P} \quad \text{(B7)}$$

PeerJ PrePrints

PeerJ PrePrints | http://dx.doi.org/10.7287/peerj.preprints.443v3 | CC-BY 4.0 Open Access | received: 12 Aug 2014, published: 12 Aug

Glossary

Nomenclature

PO_2	partial pressure of oxygen
P_{50}	partial pressure at 50% saturation
SO_2	oxygen saturation
C_{ATP}	ATP concentration
slp	slip velocity
v_p	blood plasma velocity
v_{RBC}	red blood cell velocity
H_T	tube hematocrit
$[Hb_T]$	total heme concentration
K_p	O_2 solubility in plasma
K_{RBC}	O_2 solubility in RBCs

PeerJ PrePrints

PeerJ PrePrints | http://dx.doi.org/10.7287/peerj.preprints.443v3 | CC-BY 4.0 Open Access | received: 12 Aug 2014, published: 12 Aug

K_m	O_2 Solubility in Porous Membrane
D_p	O_2 diffusivity in plasma
D_{ATP}	diffusion coefficient of ATP
D_m	O_2 Diffusivity in O_2 Permeable Membrane
N	Hill coefficient
R	ATP release rate
t	time t
n	normal unit vector
z	axial coordinate measured from channel/tube entrance
y	channel height coordinate or radial coordinate measured from tube axis
L	length of channel/tube
H	height of channel/tube

PeerJ PrePrints

PeerJ PrePrints | http://dx.doi.org/10.7287/peerj.preprints.443v3 | CC-BY 4.0 Open Access | received: 12 Aug 2014, published: 12 Aug

References

[1]Klingenberg, M., 1980, " The ADP-ATP translocation in mitochondria, a membrane potential controlled transport." J. membrane Biol., **56**, pp. 97-105.

[2] Mitchell, P., 1966,"Chmiosmotic coupling in oxidative and photosynthetic phosphorylation," Physiol Rev., **41**, pp. 445-502.

[3] Ellsworth, M.L., Ellis, C.G., Goldman, D., Stephenson, A.H., Dietrich, H.H., et al., 2009, "Erythrocytes: Oxygen sensors and modulators of vascular tone," Physiology(Betheseda), **24(2)** pp. 107-118.

[4] Dietrich, H.H., Ellsworth, M.L., Sprague, R.S., and Dacey, R.G., 2000, "Red blood cell regulation of microvascular tone through adenosine triphosphate," Am J Physiol-Heart C, **278(4),** H1294.

[5] Moschandreou, T.E., Ellis, C.G., and Goldman, D., 2011, "Influence of tissue metabolism and capillary oxygen supply on arteriolar oxygen transport: A computational model," Math Biosci, **232(1)**, pp. 1–10.

[6] Sove, R.J., Ghonaim, N., Goldman, D., Ellis, C.G., 2013, "A Computational Model of a Microfluidic Device to Measure the Dynamics of Oxygen-Dependent ATP Release from Erythrocytes," PLoS ONE, **8(11),** pp. 1-9.

[7] Moschandreou, T.E., 2012, "Blood Cell- An overview of studies in hematology": Chapter 9,"RBC-ATP Theory of regulation for tissue oxygenation-ATP concentration model, ", Intech.

PeerJ PrePrints | http://dx.doi.org/10.7287/peerj.preprints.443v3 | CC-BY 4.0 Open Access | received: 12 Aug 2014, published: 12 Aug

[8] Erkal, J.L., Selimovic, A., Gross, B.C., Lockwood, S.Y., Walton, E.L., McNamara, S., Martin, R.S., and Spence., D.M., 2014, " 3D printed microfluidic devices with integrated versatile and reusable electrodes," Lab on a Chip, Miniturization for chemistry, physics, biology, materials science and engineering, Advance Article, DOI:10.1039/C4LC00171K.

[9] Fatoyinbo, H.O., 2013," Microfluidic devices for cell manipulation,"(Edited by Li., X., and Zhou, Y.,: " Microfluidic devices for biomedical applications," pp. 283-293.

[10] Gross, B.C., Erkal, J.L., Lockwood, S.Y., Chen C., and Spence, D.M., 2014, "Evaluation of 3D printing and it's potential impact on biotechnology and the chemical sciences," Anal Chem, **86(7)**, pp. 3240-3253.

[11] Waldbaur, A., Rapp, H., Lange, K., and Rapp, B.E., 2011, "Let there be chip-towards rapid prototyping of microfluidic devices: one-step manufacturing processes," Anal Methods, **3(12)**, pp. 2681-2716.

[12] Maple 13, www.maple.ca/

[13] COMSOL Multiphysics, www.comsol.com.

[14] Nair, P.K., Huang, N.S., Hellums, J.D., and Olson, J.S., 1990, "A simple model for prediction of oxygen transport rates by flowing blood in large capillaries," Microvasc. Res., **39**,pp. 203-211.

[15] Nair, P.K.,Hellums,J.D.,and Olson, J.S., 1989, "Prediction of oxygen transport rates in blood flowing in large capillaries," Microvasc. Res., **38**, pp. 269-285.

[16] Nair, P.K., 1988, "Simulation of oxygen transport in capillaries," Thesis, Rice University.

[17] Sinha, R., 1936, Kolloid Z., **76**, pp.16-24.

[18] Pries, A.R., Secomb, T.W., and Gaehtgens, P., 1996,"Biophysical aspects of blood flow in the microvasculature," Cardiovascular Research, **32**, pp. 654-667.

[19] Mayrovitz, H.N., Larnard, D., and Duda, G., 1981, "Blood velocity measurement in human conjunctival vessels," Cardiovascular Diseases, Bulletin of the Texas Heart Institute, **8 (4),** pp. 509-526.

[20] Pries, A.R., Neuhaus, D., and Gaehtgens, P., 1992, "Blood viscosity in tube flow: dependence on diameter and hematocrit," American Journal of Physiology-Heart and Circ. Physiol., **263**, pp. H1770-H 1778.

PeerJ PrePrints | http://dx.doi.org/10.7287/peerj.preprints.443v3 | CC-BY 4.0 Open Access | received: 12 Aug 2014, published: 12 Aug

[21] Arciero, J.C., Carlson, B.E., and Secomb, T.W., 2008, " Theoretical model of metabolic blood flow regulation:roles of ATP release by red blood cells and conducted responses," Am J. Physiol Heart C Physiol, **295(4),** pp. H1582-H1571.

[22] Goldman, D.,2008,"Theoretical models of microvascular oxygen transport to tissue," Microcirculation, **15,** pp. 795-811.

[23]Goldman, D., and Popel, A.S.,2001, "A computational study of the effect of vasomotion on oxygen transport from capillary networks," J.theor. Biol., **209**,pp. 189-199.

[24] Rakel, R.E., Rakel,D.P., 2011, Textbook of family medicine, Eighth edition, Elsevier Saunders, pp. 187

[25]Dijkhuizen, P.,Buursma, A.,Fongers, T.M.E.,Gerding, A.M.,Oeseburg,B., and Zijlstra, W.G., 1977, " The oxygen binding capacity of human haemoglobin," Pflugers Archiv, **369(3)**, pp. 223-231.

PeerJ PrePrints

PeerJ PrePrints | http://dx.doi.org/10.7287/peerj.preprints.443v3 | CC-BY 4.0 Open Access | received: 12 Aug 2014, published: 12 Aug

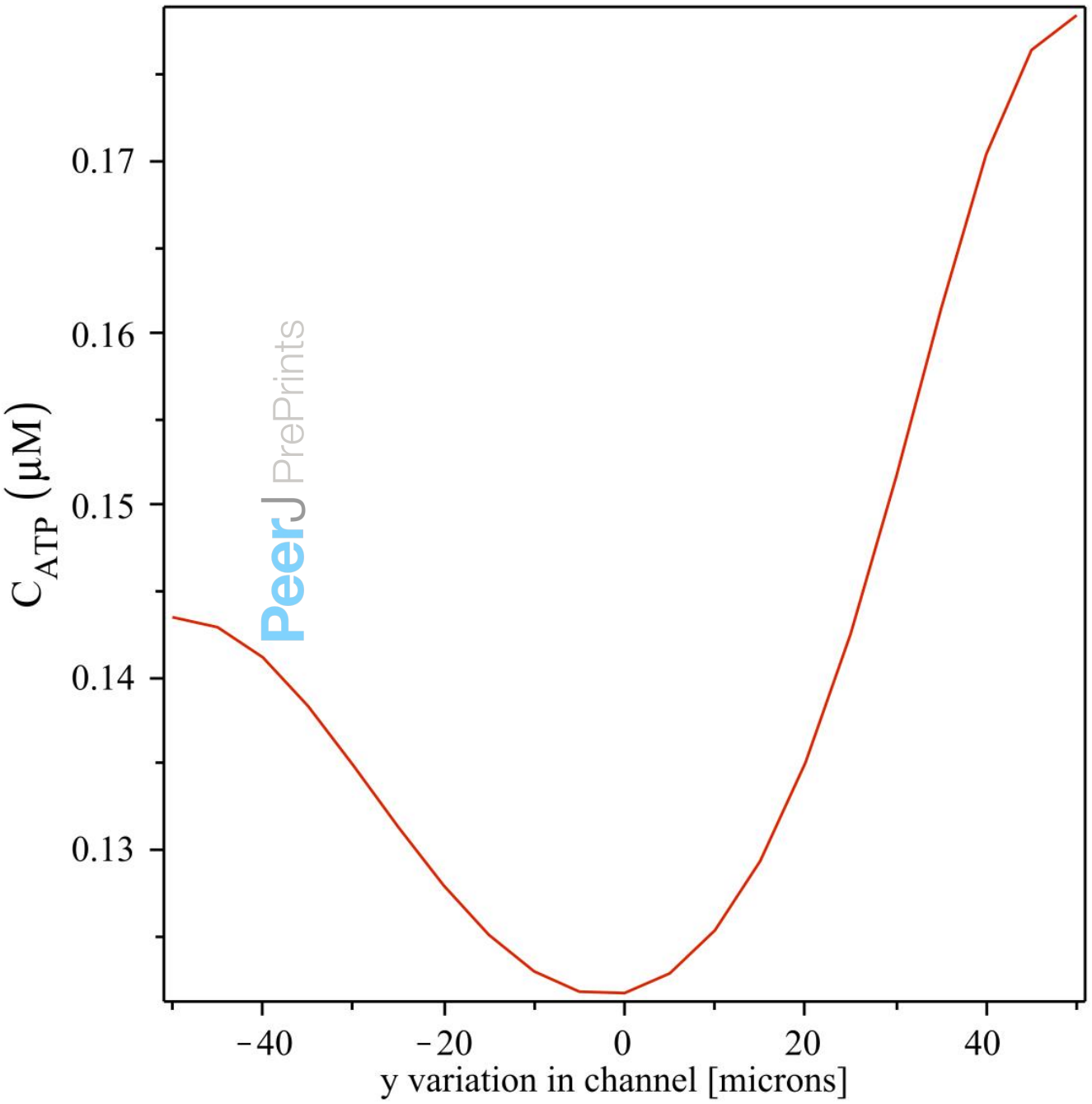

PeerJ PrePrints

PeerJ PrePrints | http://dx.doi.org/10.7287/peerj.preprints.443v3 | CC-BY 4.0 Open Access | received: 12 Aug 2014, published: 12 Aug

Figure 3-A -1 : ATP concentration versus y variation in channel at right end of permeable membrane.

PeerJ PrePrints

PeerJ PrePrints | http://dx.doi.org/10.7287/peerj.preprints.443v3 | CC-BY 4.0 Open Access | received: 12 Aug 2014, published: 12 Aug

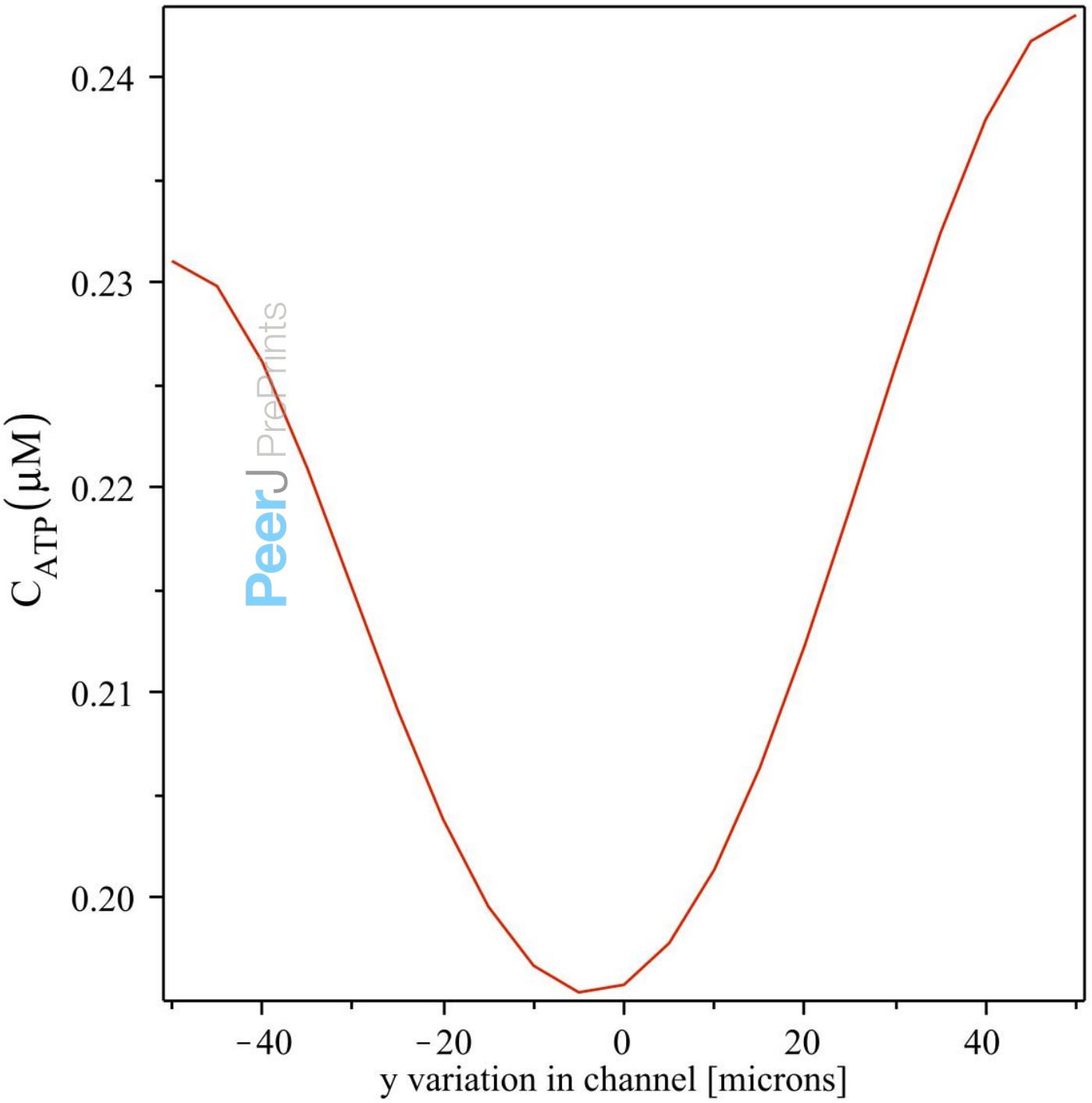

PeerJ PrePrints

PeerJ PrePrints | http://dx.doi.org/10.7287/peerj.preprints.443v3 | CC-BY 4.0 Open Access | received: 12 Aug 2014, published: 12 Aug

Figure 3-A -2 : ATP concentration versus y variation in channel, 3mm right and downstream of the end of permeable membrane.

PeerJ PrePrints

PeerJ PrePrints | http://dx.doi.org/10.7287/peerj.preprints.443v3 | CC-BY 4.0 Open Access | received: 12 Aug 2014, published: 12 Aug

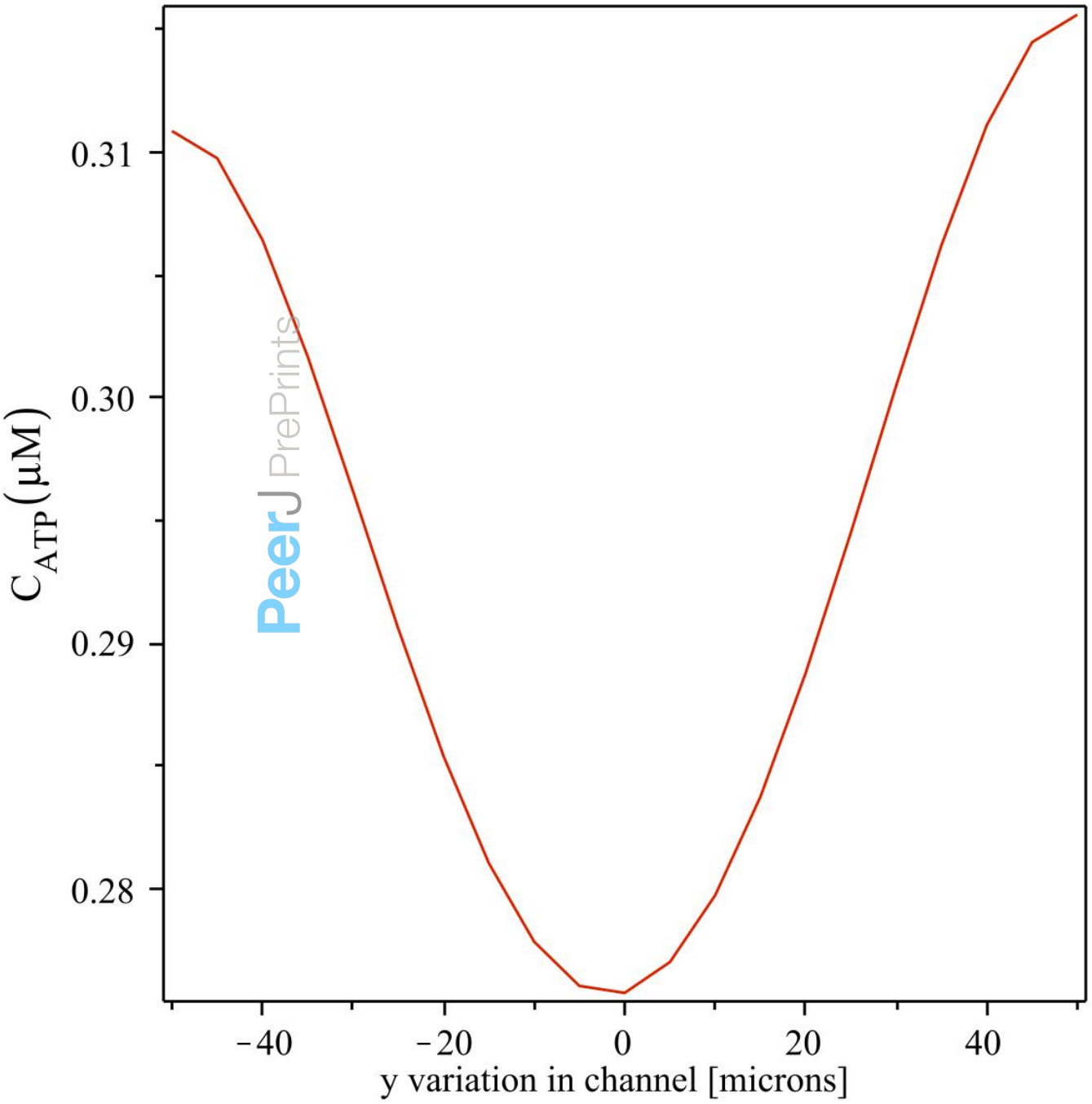

PeerJ PrePrints

PeerJ PrePrints | http://dx.doi.org/10.7287/peerj.preprints.443v3 | CC-BY 4.0 Open Access | received: 12 Aug 2014, published: 12 Aug

Figure 3-A -3 : ATP concentration versus y variation in channel, 6 mm right and downstream of the end of permeable membrane.

PeerJ PrePrints

PeerJ PrePrints | http://dx.doi.org/10.7287/peerj.preprints.443v3 | CC-BY 4.0 Open Access | received: 12 Aug 2014, published: 12 Aug

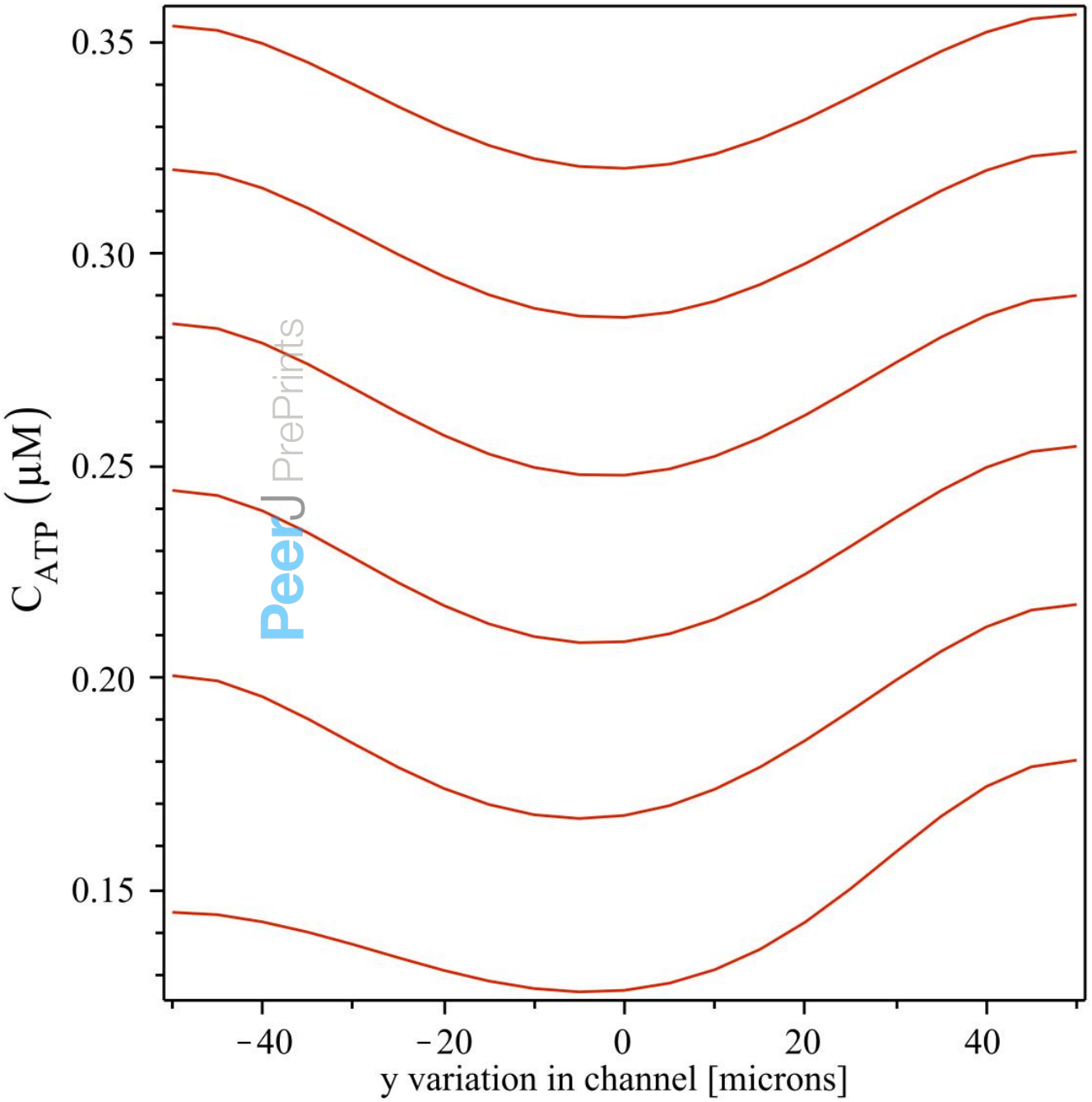

PeerJ PrePrints

PeerJ PrePrints | http://dx.doi.org/10.7287/peerj.preprints.443v3 | CC-BY 4.0 Open Access | received: 12 Aug 2014, published: 12 Aug

Figure 3-B – ATP concentration , versus y variation in channel, from membrane to far downstream from right end of membrane.

PeerJ PrePrints

PeerJ PrePrints | http://dx.doi.org/10.7287/peerj.preprints.443v3 | CC-BY 4.0 Open Access | received: 12 Aug 2014, published: 12 Aug

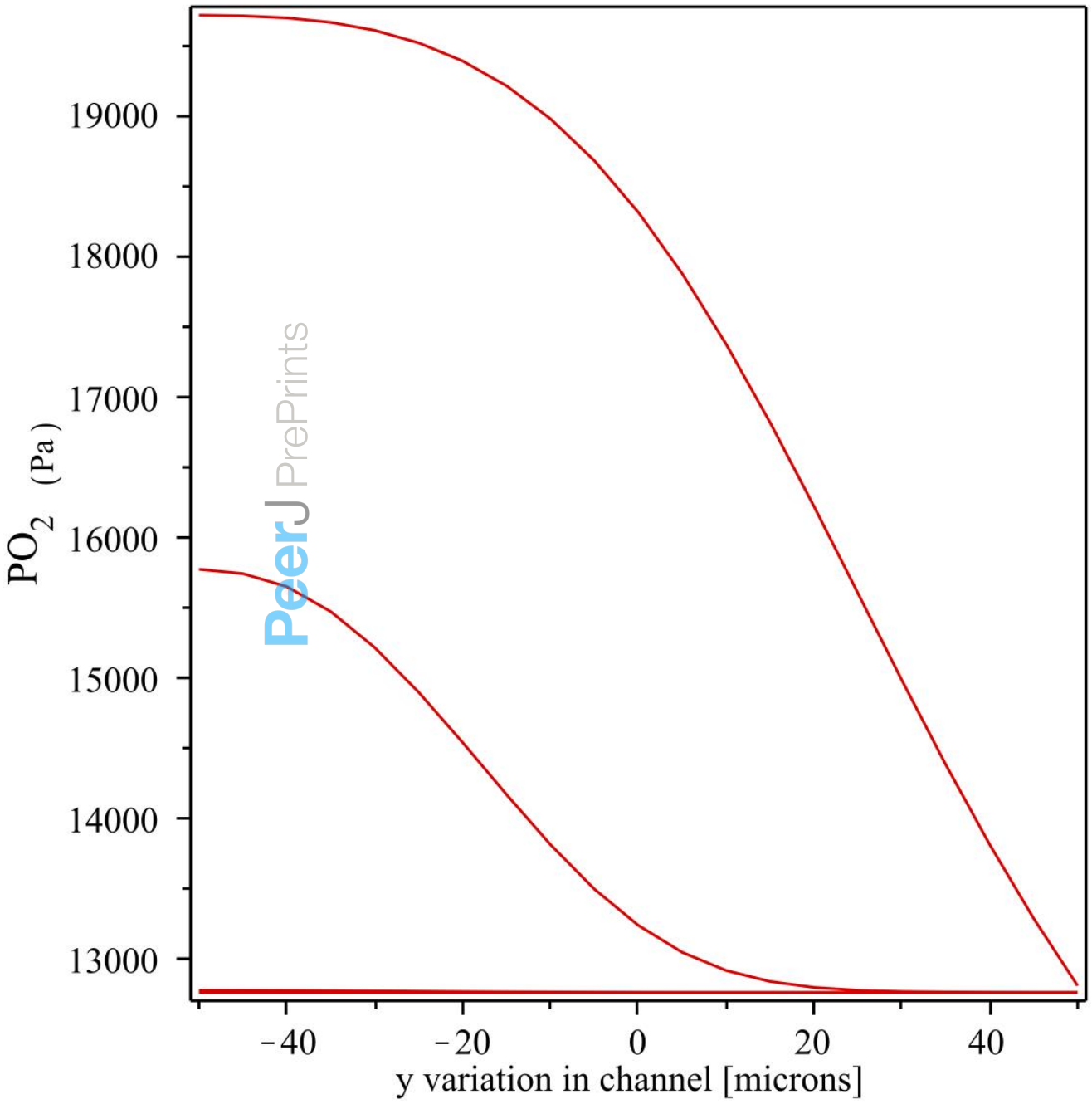

PeerJ PrePrints

PeerJ PrePrints | http://dx.doi.org/10.7287/peerj.preprints.443v3 | CC-BY 4.0 Open Access | received: 12 Aug 2014, published: 12 Aug

Figure 3-C –Oxygen tension versus y variation from membrane to downstream location in channel

PeerJ PrePrints

PeerJ PrePrints | http://dx.doi.org/10.7287/peerj.preprints.443v3 | CC-BY 4.0 Open Access | received: 12 Aug 2014, published: 12 Aug

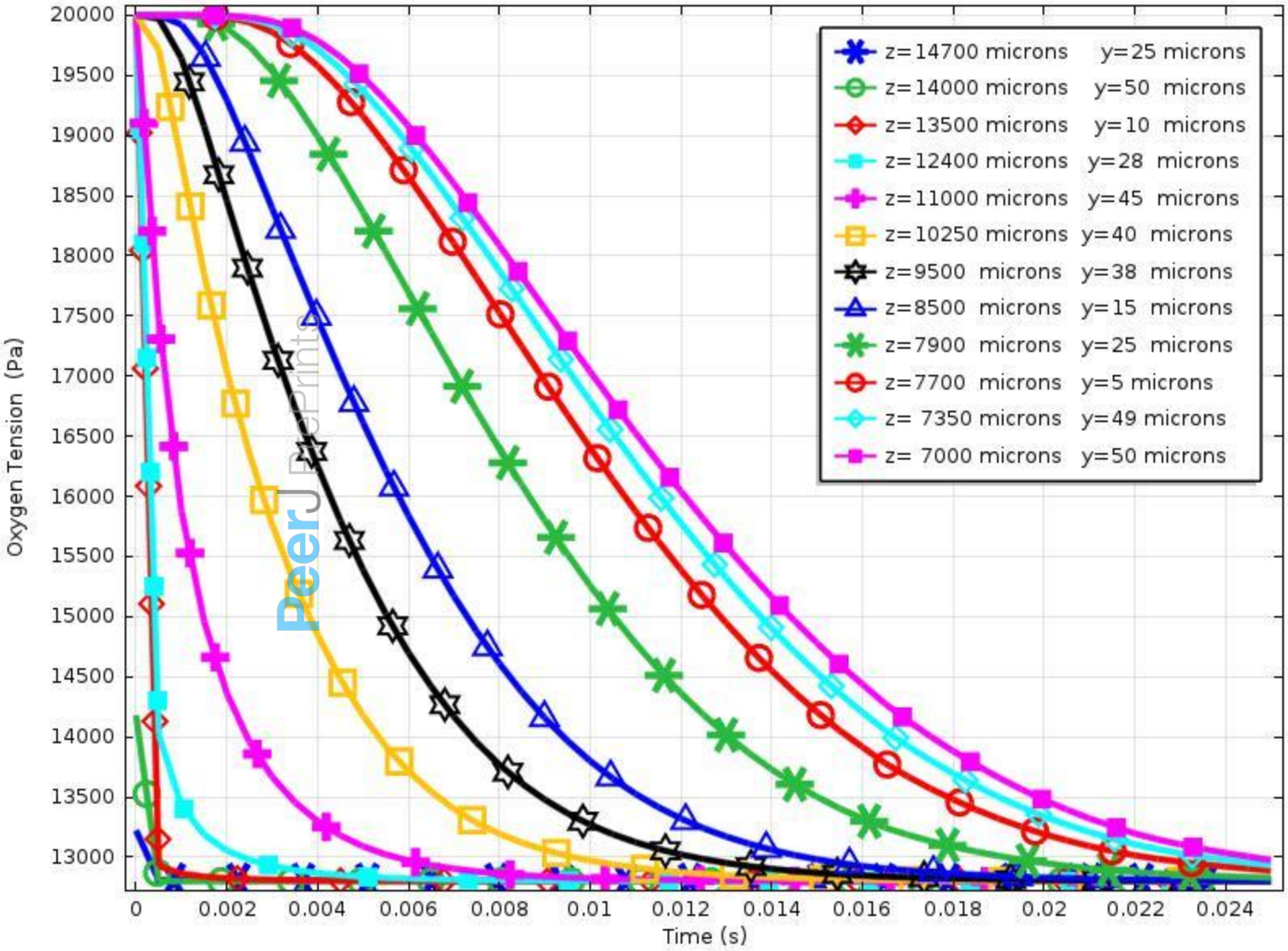

Figure 4 – Oxygen tension, versus time in seconds near permeable membrane and downstream from right end of membrane.

At various locations downstream/

PeerJ PrePrints | http://dx.doi.org/10.7287/peerj.preprints.443v3 | CC-BY 4.0 Open Access | received: 12 Aug 2014, published: 12 Aug

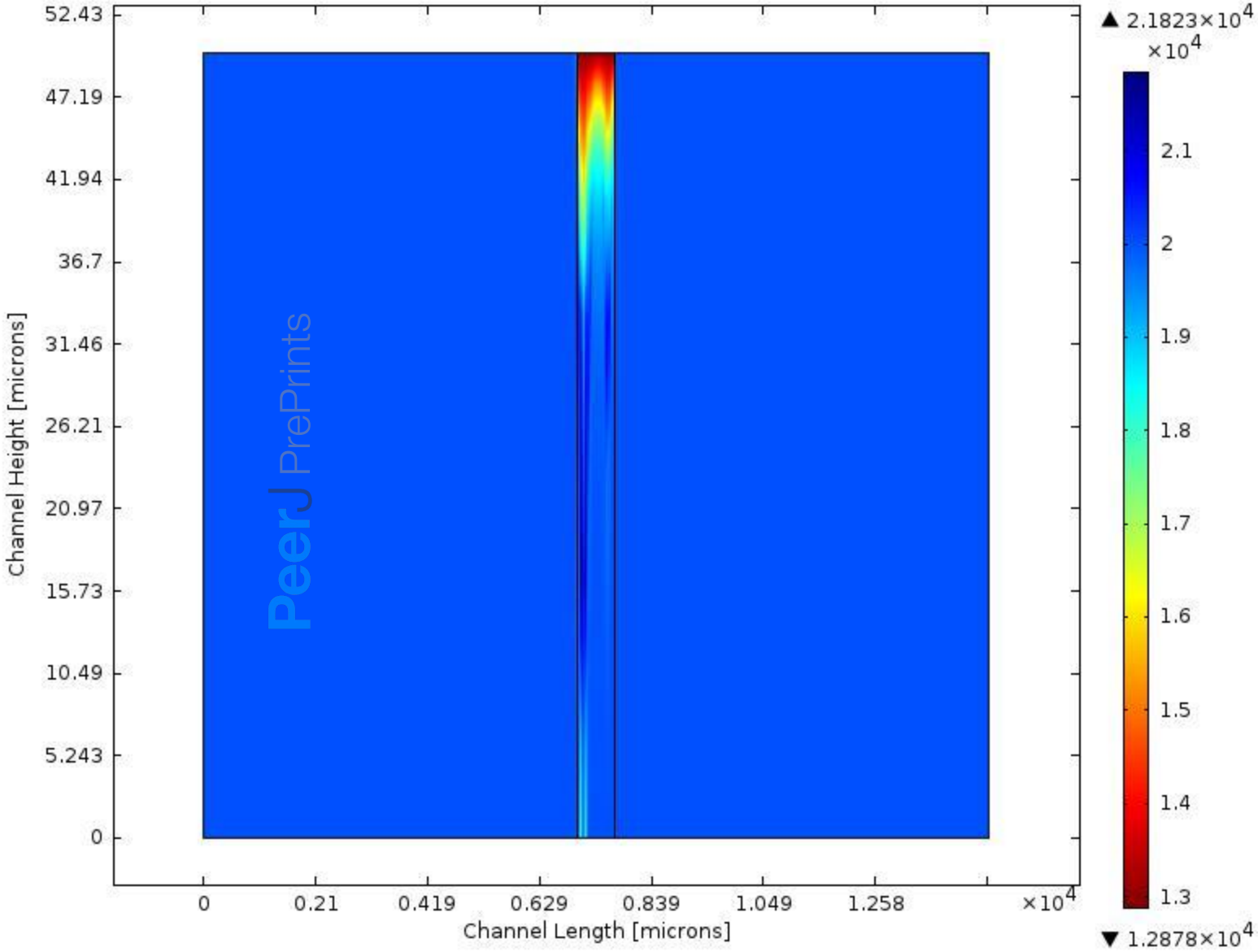

Figure 5- Oxygen tension distribution in channel for present study, at time t= 5e-5 seconds.

PeerJ PrePrints | http://dx.doi.org/10.7287/peerj.preprints.443v3 | CC-BY 4.0 Open Access | received: 12 Aug 2014, published: 12 Aug

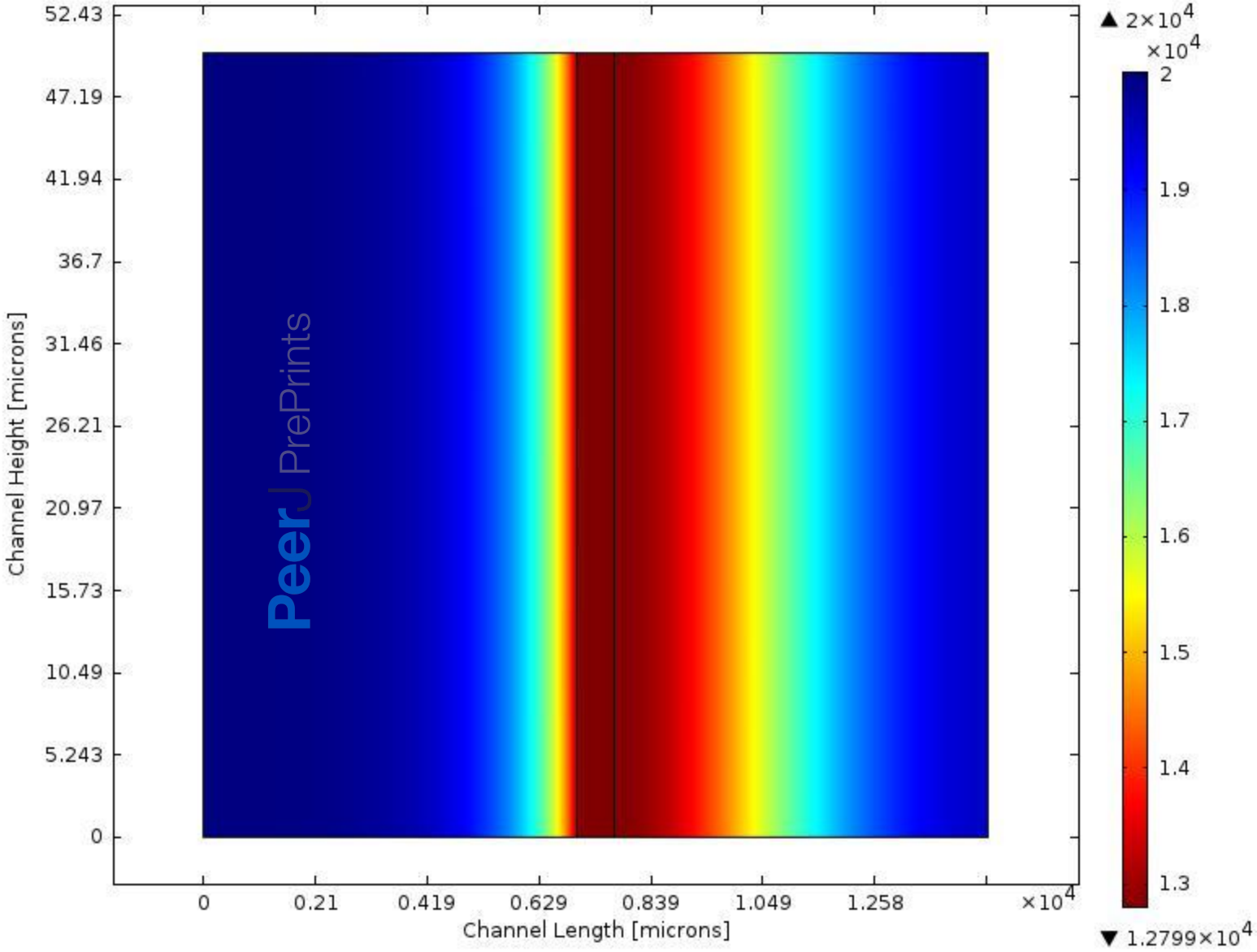

Figure 6- Oxygen tension distribution in channel for present study, at time t= 0.005 seconds.

PeerJ PrePrints | http://dx.doi.org/10.7287/peerj.preprints.443v3 | CC-BY 4.0 Open Access | received: 12 Aug 2014, published: 12 Aug

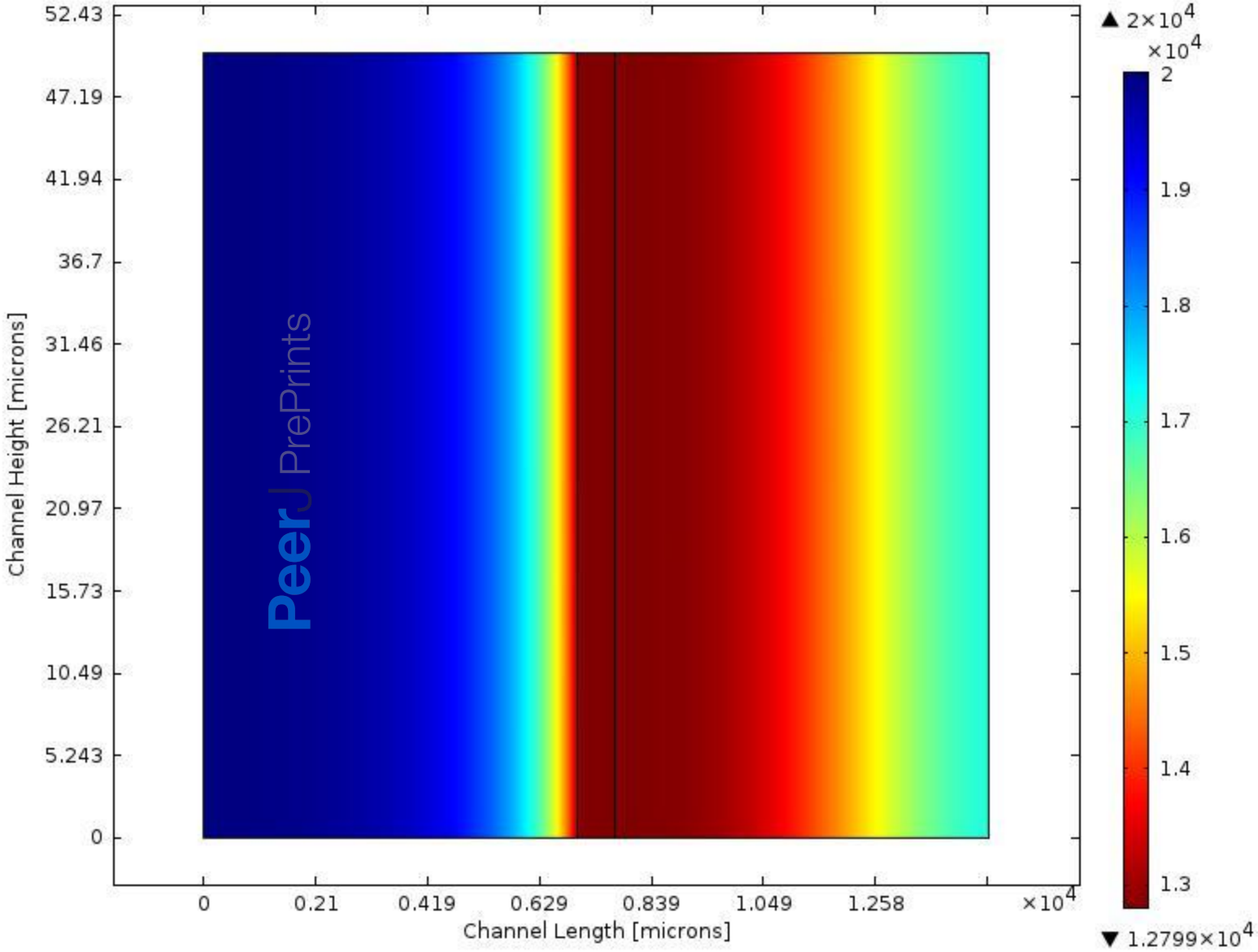

Figure 7- Oxygen tension distribution in channel for present study, at time t= 0.01 seconds.

PeerJ PrePrints | http://dx.doi.org/10.7287/peerj.preprints.443v3 | CC-BY 4.0 Open Access | received: 12 Aug 2014, published: 12 Aug

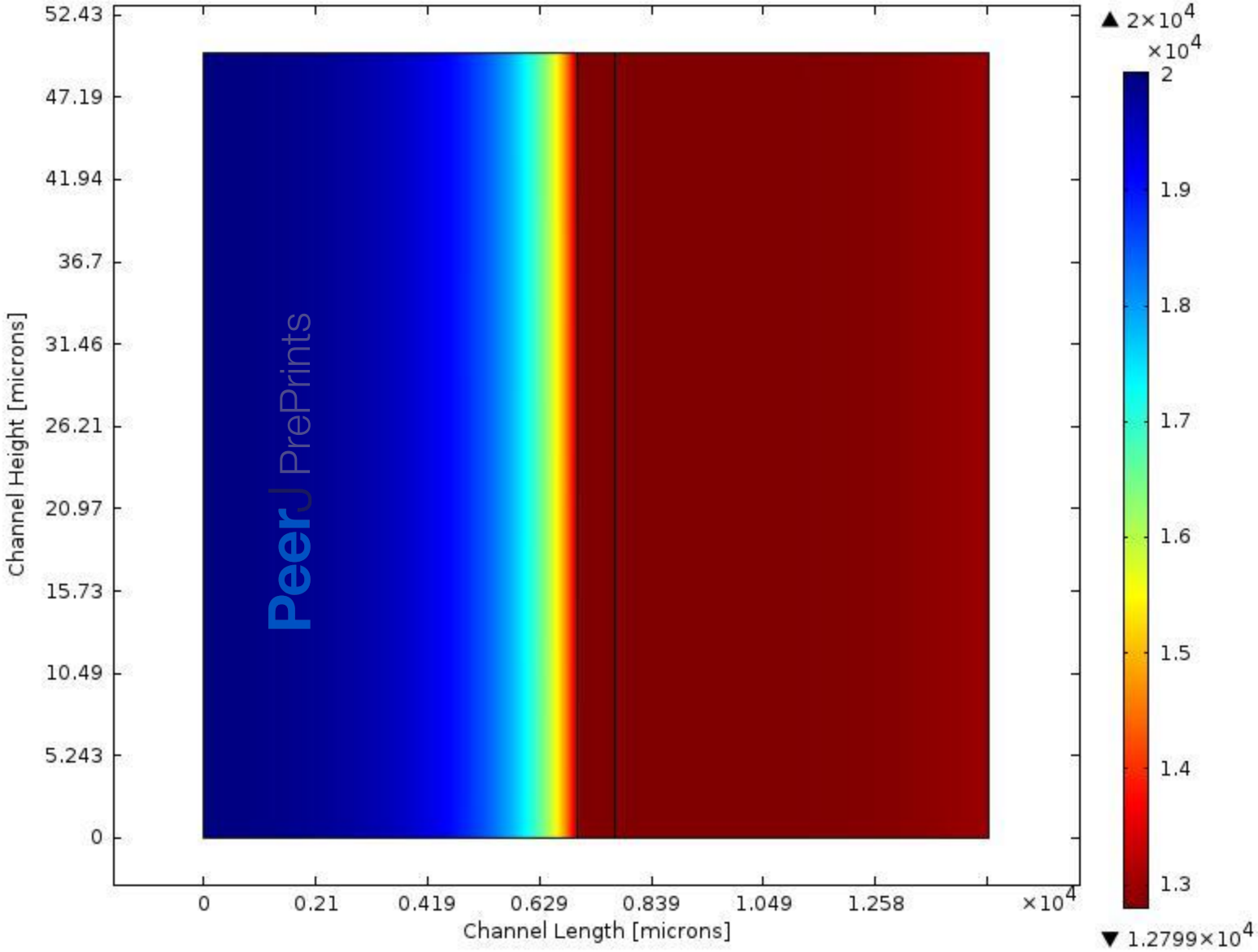

Figure 8- Oxygen tension distribution in channel for present study, at time t= 0.025 seconds.

PeerJ PrePrints | http://dx.doi.org/10.7287/peerj.preprints.443v3 | CC-BY 4.0 Open Access | received: 12 Aug 2014, published: 12 Aug